NASA/TM–2011-217048

Method and Apparatus for the Quantification of Particulate Adhesion Forces on Various Substrates

Christopher J. Wohl
Langley Research Center, Hampton, Virginia

Brad M. Atkins
Rhodes College, Memphis, Tennessee

John W. Connell
Langley Research Center, Hampton, Virginia

February 2011

NASA STI Program . . . in Profile

Since its founding, NASA has been dedicated to the advancement of aeronautics and space science. The NASA scientific and technical information (STI) program plays a key part in helping NASA maintain this important role.

The NASA STI program operates under the auspices of the Agency Chief Information Officer. It collects, organizes, provides for archiving, and disseminates NASA's STI. The NASA STI program provides access to the NASA Aeronautics and Space Database and its public interface, the NASA Technical Report Server, thus providing one of the largest collections of aeronautical and space science STI in the world. Results are published in both non-NASA channels and by NASA in the NASA STI Report Series, which includes the following report types:

- TECHNICAL PUBLICATION. Reports of completed research or a major significant phase of research that present the results of NASA programs and include extensive data or theoretical analysis. Includes compilations of significant scientific and technical data and information deemed to be of continuing reference value. NASA counterpart of peer-reviewed formal professional papers, but having less stringent limitations on manuscript length and extent of graphic presentations.

- TECHNICAL MEMORANDUM. Scientific and technical findings that are preliminary or of specialized interest, e.g., quick release reports, working papers, and bibliographies that contain minimal annotation. Does not contain extensive analysis.

- CONTRACTOR REPORT. Scientific and technical findings by NASA-sponsored contractors and grantees.

- CONFERENCE PUBLICATION. Collected papers from scientific and technical conferences, symposia, seminars, or other meetings sponsored or co-sponsored by NASA.

- SPECIAL PUBLICATION. Scientific, technical, or historical information from NASA programs, projects, and missions, often concerned with subjects having substantial public interest.

- TECHNICAL TRANSLATION. English-language translations of foreign scientific and technical material pertinent to NASA's mission.

Specialized services also include creating custom thesauri, building customized databases, and organizing and publishing research results.

For more information about the NASA STI program, see the following:

- Access the NASA STI program home page at *http://www.sti.nasa.gov*

- E-mail your question via the Internet to help@sti.nasa.gov

- Fax your question to the NASA STI Help Desk at 443-757-5803

- Phone the NASA STI Help Desk at 443-757-5802

- Write to:
  NASA STI Help Desk
  NASA Center for AeroSpace Information
  7115 Standard Drive
  Hanover, MD 21076-1320

NASA/TM–2011-217048

Method and Apparatus for the Quantification of Particulate Adhesion Forces on Various Substrates

Christopher J. Wohl
Langley Research Center, Hampton, Virginia

Brad M. Atkins
Rhodes College, Memphis, Tennessee

John W. Connell
Langley Research Center, Hampton, Virginia

National Aeronautics and
Space Administration

Langley Research Center
Hampton, Virginia 23681-2199

February 2011

Acknowledgments

The authors would like to acknowledge Dr. Brent Hoffmeister from Rhodes College in Memphis, Tennessee who contributed significantly to Brad Atkins research at Rhodes College and provided a wealth of experience and advice during the construction and initial operation of the adhesion device described herein. The authors also acknowledge Dr. Michael Mullins from Michigan Technological University. Dr. Mullins was the lead author of the literature exemplar from which the adhesion device described in this work was generated. He was very forthcoming with information and exhibited a sincere interest in the "rebirth" of research he conducted in the past.

The authors acknowledge the NASA Langley Research Summer Scholars program hosted by the National Institute of Aerospace. This program enabled Brad Atkins to conduct research at NASA Langley for two summers and also facilitated research he conducted during an entire academic year at Rhodes College in Memphis, Tennessee.

The authors also acknowledge funding from the Creative and Innovative (C&I) research program at NASA Langley Research Center directed by Dennis Bushnell. This program provided great liberty to pursue the research interests of the authors as they related to lunar dust adhesion mitigation and the device described herein was procured, assembled, and operated with funding exclusively from the C&I program.

The authors also acknowledge the patience and assistance of Dr. Jeffrey Hinkley from NASA Langley's Advanced Materials and Processing Branch. Dr. Hinkley contributed his time and expertise to analysis of the data and connection with fundamental material properties.

Available from:

NASA Center for AeroSpace Information
7115 Standard Drive
Hanover, MD 21076-1320
443-757-5802

Introduction

The timely and successful completion of lunar surface missions, manned or unmanned, will require overcoming several technical challenges. One of several significant challenges identified by NASA that could negatively impact mission operations is the presence of lunar dust.[1-6] The lunar dust, comprising approximately 50% of the lunar regolith, is the fines portion with particulate diameters ≤ 60 μm.[7] Due to its size, surface topography, and material properties, the lunar dust adheres strongly to exposed surfaces.[8,9] These attributes are a result of the processes responsible for lunar dust generation. Micrometeoroid bombardment causes the fracturing and agglutination of lunar regolith, and has been associated with the formation of nanophase iron (Fe^0) deposits.[10] This results in the formation of porous particles with sharp asperities. Additionally, exposure to UV and other energetic species results in electrostatic charging of the lunar dust[11-14] which can lead to even greater adhesive forces. Combined, these properties introduced several difficulties during the Apollo missions including the abrasion of visors, gloves, and boots, degradation of seals and thermal radiator performance, and respiratory distress.[15,16] Recently, the retro-reflectors deposited on the lunar surface have exhibited a decrease in signal intensity of a factor of ten.[17] The probable source of this degradation is the accumulation of lunar dust on the retro-reflectors' surface. For these difficulties to be minimized or mitigated, novel materials and related technologies will need to be developed to both passively and actively eliminate lunar dust adhesion.[18-21]

As new materials and technologies are developed to minimize the impact of lunar dust on exposed surfaces, methods need to be developed that analytically assess and quantitatively evaluate these approaches. Since the environmental conditions on the lunar surface and the complex combination of properties possessed by lunar dust cannot be reproduced in terrestrial laboratories, correlations need to be established between terrestrial properties and measurements, and the predicted performance on the lunar surface. For active mitigation strategies, such as electrodynamic dust screens,[22] testing the efficacy of the technology is an imperative step in the technology development process and will therefore follow a very straightforward approach. For passive mitigation strategies (i.e., generation of low surface energy materials) the evaluation process is much less obvious. An example of a passive approach to lunar dust adhesion mitigation would be the research at NASA Langley Research Center's Advanced Materials and Processing Branch, which has focused on mitigating particulate adhesion through lowering the surface energy of materials both chemically and topographically.[18] Crude methods, such as surface particulate coating and inverting tests or insertion and removal of substrates from particulate filled containers,[23] can be useful and may even offer insight into the efficacy of the tested material, but these subjective tests produce results that are difficult to correlate.

Sonic particle detachment offers benefits of both qualitative and quantitative adhesion testing techniques. Similar to inversion tests, coating of a material with a large number of particles enables determination of surface clearance with many-body interactions. Likewise, adhesion forces can be calculated as a function of applied force comparable to that of atomic force microscopy (**AFM**).[25,26] Sonic particle detachment can also surmount AFM's constraint to measure forces between a cantilever tip and surface rather than actual particulates. Although cantilevers can be modified via chemical modification of the surface or affixing objects to the tip itself, the processes can be extremely difficult and introduce an array of challenges that need to be overcome to obtain meaningful data.[27-30] Sonic detachment studies can be correlated to inexpensive and routine screening techniques such as contact angle goniometry that permit the assessment of surface engineered materials.

This report describes the generation and performance of a method and an instrument to evaluate the adhesion of particulates to surfaces of interest. An adhesion testing device, based on a literature exemplar,[24] was used to agitate a surface coated with a monolayer of particles. The surface was suspended over an optical particle counter that counted the particles as they were gravitationally fed into

the analytical window. Through precise control of the magnitude of sonic wand tip actuation and quantitative determination of the number of particles removed from and remaining on the surface at the end of the experimental procedure, adhesion force values were calculated. Materials with minimal particle adhesion forces would presumably be preferential for lunar surface applications.

To ascertain the efficacy of surfaces for lunar dust adhesion mitigation, the forces involved with adhesion need to be described. Therefore, what follows is a brief description of the detachment force acting on adhered particles as a result of the sonic wand actuation followed by a brief analysis of the theory developed for particle substrate interaction forces as they relate to the work of adhesion. Next, the materials studied, details of instrument generation, and a description of the processes developed for data analysis are explained. Finally, preliminary results are described and additional thoughts are provided regarding incorporation of electric field and UV generation devices as an approach better emulate the lunar surface environment.

Particle Detachment via Sonication

Since the adhesion forces of particulates the size of lunar dust can greatly exceed their earth or in situ lunar gravitational forces, detachment techniques using substrate surface vibration necessitate relatively large displacement at high accelerations. These acceleration rates may be achieved using ultrasonic equipment where controlled oscillation is applied to a sample pre-coated with an approximate monolayer of particulates. For the experiments described here, the frequency of oscillation was kept constant, 20 kHz, while amplitude was adjusted in controlled step-wise intervals from device minimum to maximum. This process was designed to result in detachment of particles from the sample substrate when the mechanical force arising from sonic wand device vibration overcame the particulate-substrate adhesion force. With knowing the particle's size, the detachment force can be computed directly from Newton's relationship:

$$F_{Detach} = ma \tag{1}$$

where m is the mass of a particle and a, the surface acceleration is computed from:[31]

$$a = 4\pi^2 f^2 A \tag{2}$$

where f and A denote the frequency and amplitude of oscillation, respectively. This relationship assumes that the change in acceleration of the sonic wand follows a sinusoidal pattern.

Particle Adhesion Theory

A standard first approximation in the field of particulate adhesion is to model interaction between particles and a sample material surface using van der Waals' equation for adhesion force between a sphere and a planar surface:

$$F_{vdW} = (H'R)/(6d_0^{\,2}) \tag{3}$$

where H' is:

$$H' = (H_1 H_2)^{1/2} \tag{4}$$

where R is the radius of particulate, and d_o is the interfacial cut-off distance at which atomic repulsion occurs, H' represents the averaged Hamaker constant, and H_1 and H_2 are the Hamaker constants for the particulate and substrate, respectively. In the studies described here d_o = 0.165 nm.[32] Passive adhesion mitigation strategies consist of reducing surface energy and generating surface topographies on materials in order to reduce van der Waals interactions.

There are several different approaches and theories that can be used to determine the work of adhesion, W_a, from adhesion force values. Hertz theory was developed with the assumption that there were no surface forces between the particle and the substrate and the contact geometry was maintained. Thus only van der Waals forces needed to be surmounted.[33] The Johnson-Kendall-Roberts theory (**JKR**) was developed as an extension of Hertz theory. JKR considered the interactions between the particle and the surface within the contact area, and allowed modification of the contact geometry as a result of these forces.

According to JKR theory, the adhesion force can be related to the work of adhesion by:

$$F_{adh} = \frac{3}{2}\pi R W_a \tag{5}$$

The work of adhesion can then be used to calculate the contact radius, a_o, of particles adhered to the surface according to:

$$a_0 = \left(\frac{6\pi R^2 W_a}{K} \right)^{1/3} \tag{6}$$

where K is:

$$K = \left(\frac{4}{3} \right) \left(\frac{1-\nu_1^2}{E_1} + \frac{1-\nu_2^2}{E_2} \right)^{-1} \tag{7}$$

Thus, the contact radius and ultimately the work of adhesion depend upon the Poisson's ratio, ν_i, and the elastic modulus, E_i, of both the substrate and the particle. This value can be compared with the particle size to determine an embedding depth of particles on the surface. To determine the embedding depth, a right triangle can be envisioned consisting of sides defined as; r (contact radius), R (particle radius), and x as illustrated above. Using the Pythagorean theorem, the value of x can be readily determined. Thus the embedding depth, h, can be calculated by subtracting x from the particle radius. This assumes that there is no significant deformation of the particle upon adhesion.

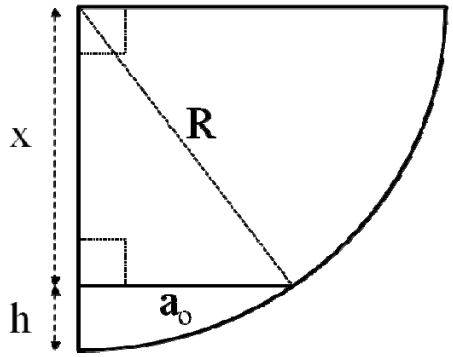

Materials and Methods

Particulates Studied:

The adhesion studies described here have largely focused on using rigid spherical particulates as an effort to minimize experimental variables such as differences in particle shape, porosity, and composition.

The particulates used were soda-lime glass particles (diameters from 10 – 70 microns) that have similar size domain, chemical composition and electrical conductivity as lunar simulant (NASA/USGS Lunar Highlands Simulant), making them excellent candidates for this adhesion study. The relevant mechanical properties (obtained from Valley Design Corp.) of the particulates and substrates studied here are detailed in Table 1. The Hamaker constants for all of the materials investigated here were obtained from literature sources.[34]

Substrates Studied:

To ascertain the efficacy of the adhesion testing device, substrates with a broad range of material properties (Poisson's ratios and elastic moduli) were investigated (Table 1). A series of substrates were selected based on differences in surface energy. The sonic wand tip, fabricated from titanium alloy Ti-6Al-4V (Aerospace Specification Metals Inc.), was investigated due to the differences in mechanical properties compared with the other substrates investigated here. A commercially available polyimide, Kapton® HN (Dupont de Nemours and Corp.) was investigated and the mechanical properties indicated in Table 1 were obtained from the manufacturer. A copoly(imide siloxane) (**PIS**) generated from 4,4'-oxydiphthalic anhydride (ODPA), 4,4'-oxydianiline (4,4'-ODA), and an amine-terminated siloxane (a surface modifying agent, DMS-A21, 6100 g mol^{-1}, Gelest Inc., 1 wt. %) were also studied. The copoly(imide siloxane) material was synthesized in a manner similar to that described in ref. 18.

A two-part silicone material, Silastic T2, (Dow Corning Corporation, mechanical properties obtained from literature)[35] was also employed to evaluate how changes in surface topography impact adhesion. Silicate materials exhibit pronounced adhesive interactions with silicones and as such should strongly adhere to Silastic T2 surfaces. To evaluate changes in surface topography, Silastic T2 material was molded against a laser ablation patterned aluminum substrate. The aluminum was patterned with a frequency-tripled Nd:YAG laser (λ = 355 nm) using a 90° cross-hatch pattern resulting in an approximate square pillar array with feature width, height, and pitch of 25 μm, 15 μm, and 25 μm respectively. The negative of this pattern, which would be an array of 15 μm raised rectangular features with depressed central regions, was transferred to the Silastic T2 material.

Table 1. Relevant material properties for the materials and particles studied.

Material	Poisson's Ratio	Young's Modulus (GPa)	Hamaker Constant (J)
Ti-6Al-4V	0.34	114	4.0×10^{-19}[a]
Kapton®	0.34	2.5	5.0×10^{-20}
PIS	0.34[b]	2.7[c]	4.7×10^{-20}[d]
Silastic® T2	0.45	0.002	4.5×10^{-20}
Soda-lime Glass Spheres	0.22	72	3.1×10^{-20}

[a] *Average value for metallic surfaces.*
[b] *Assumed to be similar to Kapton®.*
[c] *Determined in-house.*
[d] *Taken as the geometric mean of the Kapton® and Silastic® T2 values.*

Adhesion Testing Device:

The adhesion testing apparatus was assembled from three major components; an environmental chamber, a sonication device, and an optical particle counter. The environmental chamber used in this study was an aluminum environmental chamber (0.227 m^3 cube, Abbess Instruments and Systems Inc., Holliston, MA) capable of maintaining reduced atmospheric pressures down to 10^{-4} Torr. The chamber had several feedthroughs for a variety of instruments and gas inlet valves to introduce inert atmospheres,

control humidity level, etc. The sonication device (Vibracell VCX-750, Sonics and Materials Inc., Newtown, CT) operated at 20 kHz and was capable of surface displacements (accelerations) ranging from 12.2 μm (193 km/s) to 124 μm (1960 km/s) using 12.7 mm and 19 mm tips. The optical particle counter (OPC, Solair 3100, Lighthouse Worldwide Solutions, San Jose, CA) utilized laser scattering for particle detection and was capable of measurements as low as 0.1 micron.

Although there are two possible configurations of the instrumentation within the chamber (a 'vertical' and 'horizontal' configuration) the work described here utilized the horizontal configuration exclusively, see Figure 1. In this configuration, the sonic wand tip was positioned approximately 12.7 mm above a collection cone that was connected to the optical particle counter with a minimal amount of tubing (the major drawback to the vertical configuration was the significant length of requisite tubing connecting the collection cone to the optical particle counter within the environmental chamber).

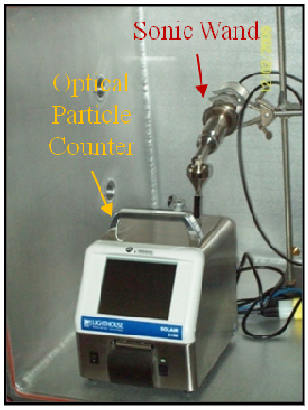

Figure 1. The adhesion device assembled in a 'horizontal' configuration.

Sample Preparation:

Samples were prepared by affixing a 6 mm circle of the substrate cut from a hole punch onto the tip of the sonication device using a cyano-acrylate adhesive (Hot Stuff, Satellite City Inc., Simi, CA). To prevent contamination of the sample surface with the adhesive, a minimal amount of the adhesive was applied to a small diameter wooden stick which was translated in a circular motion across the middle of the sonic wand tip to apply a thin coating of the adhesive. Next, the sample was placed on the adhesive-coated sonic wand tip using tweezers. (NOTE: for studies involving the sonication device tip itself, nothing was affixed to the surface.) The prepared surfaces were allowed to dry for a minimum of 2 h prior to their use in the device. In order to yield accurate and reproducible adhesion data, an approximate monolayer coating of particulate material was necessary. To achieve an approximate monolayer coating a simple aerosolization technique was developed where particulates were lofted into the free space of an enclosed container using approximately one burst-per-milligram of particles from a compressed air canister (Figure 2A). Optical microscopy was used to verify the extent of particulate coating (Figure 2B). Particle coating was restricted to the area comparable to the hole punch size and particulates deposited outside this region were carefully removed using dust free laboratory wipes (Kimwipe®, Kimtech Sciences). If significant deviation from a monolayer was observed, the sample was carefully cleaned, as verified using optical microscopy, and re-coated. Pre-sonication micrographs were taken documenting particulates deposited on the substrate, particulate coating, size of particulate, and size of sonic wand tip (12.7 mm and 19 mm). These images were compared to post-sonication images to determine the percent of surface clearance of the sample surface.

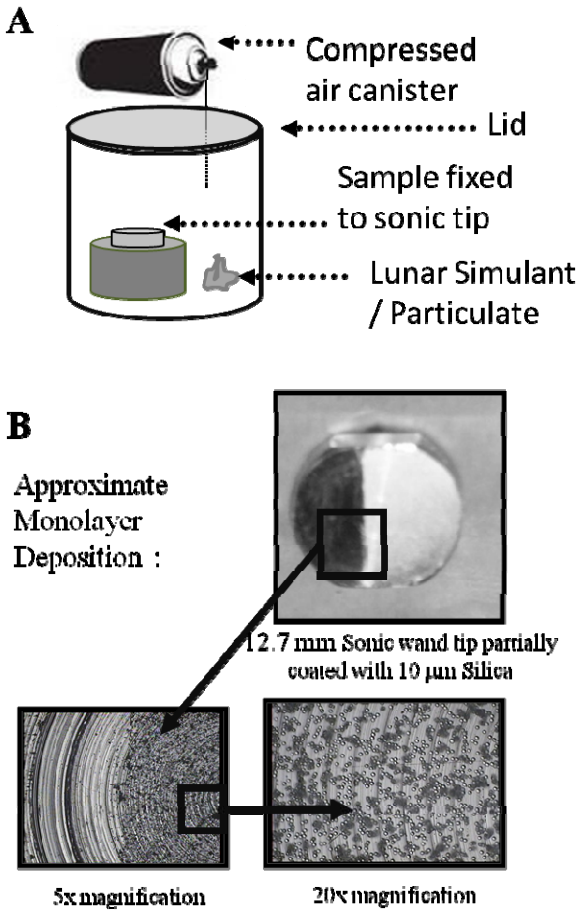

Figure 2. A) The deposition of an approximate monolayer of particles on a substrate. B) A 12.7 mm sonic wand tip partially coated with 10 µm soda-lime glass particles and 5x and 20x magnified images demonstrating a coating approximating a monolayer.

Adhesion Test Protocol:

After the sample met the coating requirements (having a sufficient monolayer) it was attached to the sonic wand device, which was positioned above the optical particle counter collection cone. The sonic wand device and OPC were turned on and data acquisition was initiated for the OPC using a real-time data collection program (LMS Express 2006 RT, Lighthouse Worldwide Solutions, San Jose, CA) provided with the instrument. A total of 60 measurements were collected for an individual experiment, each over the span of 30 seconds with a halt period of 5 seconds between measurements, partitioned as follows: 1) steps 1-4 were recorded to collect information about ambient particles within the testing chamber, 2) every following even-numbered step recorded additional ambient background particle data, while every following odd-numbered step recorded particle detachment data. The particle detachment steps involved an iterative increase in surface acceleration via an increase in percent of maximum sonic wand displacement amplitude. These measurement steps are summarized in the sample data log shown below (Table 2). The background runs and % amplitude settings are indicated for each step number. The 10 micron bin particle count column is included to insure that the data downloaded from the instrument correlates with real-time observations.

For the particle detachment steps, three brief pulses of the sonic wand, lasting approximately one second each were applied at the percentage of maximum sonic wand amplitude displacement. The optical particle counter recorded particle counts according to different 'bin' sizes which included 1, 3, 5, and 10 micron partitions that refer to the particle diameter. The bins included particle sizes up to the size of the following bin. As an example, the 3 micron bin would contain particle counts for particles ranging from 3.0 to 4.9 microns; larger particles would be counted in the 5 or 10 micron bin according to their size.

Table 2. A typical experimental schedule.

Sample											
Chamber Temperature:			Chamber Humidity:						Date:		
Step	% of Max. Amplitude	10 μm Count	**Step**	% of Max. Amplitude	10 μm Count	**Step**	% of Max. Amplitude	10 μm Count	**Step**	% of Max. Amplitude	10 μm Count
1	Background		**16**	Background		**31**			**46**	Background	
2	Background		**17**			**32**	Background		**47**		
3	Background		**18**	Background		**33**			**48**	Background	
4	Background		**19**			**34**	Background		**49**		
5			**20**	Background		**35**			**50**	Background	
6	Background		**21**			**36**	Background		**51**		
7			**22**	Background		**37**			**52**	Background	
8	Background		**23**			**38**	Background		**53**		
9			**24**	Background		**39**			**54**	Background	
10	Background		**25**			**40**	Background		**55**		
11			**26**	Background		**41**			**56**	Background	
12	Background		**27**			**42**	Background		**57**		
13			**28**	Background		**43**			**58**	Background	
14	Background		**29**			**44**	Background		**59**		
15			**30**	Background		**45**			**60**	Background	

Contact Angle Goniometry:

Sessile drop contact angles were measured for each sample using a 8 μL drop of either water or ethylene glycol, or a 2.25 μL drop of methylene iodide on an FTA 1000 contact angle goniometer (First Ten Angstroms, Portsmouth, VA). Interfacial tension measurements of a suspended drop of each liquid were made prior to experimentation to verify the purity of the liquid and precision of the focused image. Contact angles were determined by drop shape analysis and standard deviations were calculated by comparison of the contact angles observed for each frame of a 40 frame movie collected after drop deposition on the sample surface. Each sample was measured at least three times.

Results and Discussion

Data Analysis:

After completion of the adhesion testing protocol, the sample surface was imaged using optical microscopy to determine percent surface clearance. For surfaces that exhibited complete clearance, the data from the OPC was used directly. For surfaces that did not completely clear, ImageJ software was used to approximate percent clearance by determining the area of the image coated with particulate material, $Area_0$ and $Area_F$ from the optical images collected before and after the adhesion testing protocol, respectively. To perform the particle analysis, the optical micrograph samples were converted to an 8-bit gray scale image and then converted to a threshold image where the lower and upper threshold limits were set to separate the particulate material from the substrate. Size and circularity patterns were adjusted to capture particle sizes of significance for the particular study. The scaling factor, $Clear_{\%}$, was then calculated according to:

$$Clear_{\%} = \frac{(Area_0 - Area_F)}{Area_0} * 100\% \quad (8)$$

An example of ImageJ analysis for a Kapton® HN film sample attached to a small sonic wand tip is shown below (Figure 3).

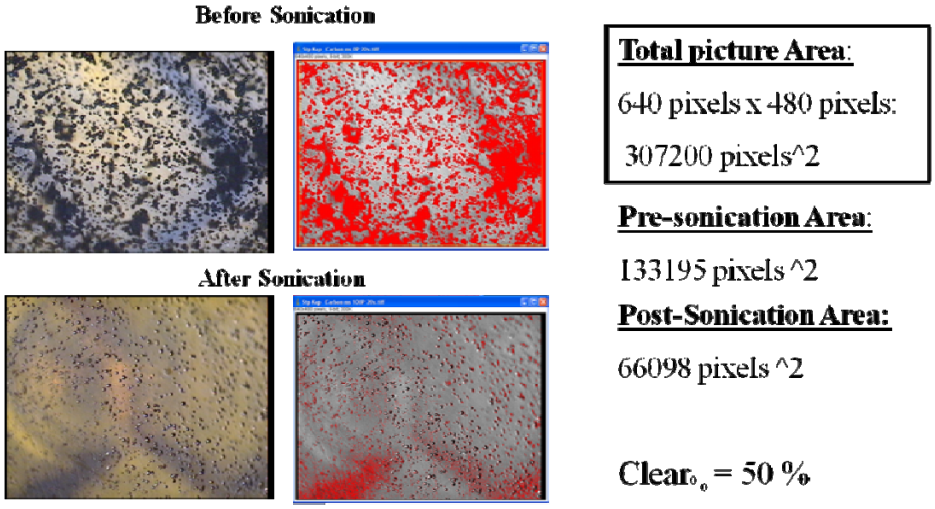

Figure 3. ImageJ analysis of the number of pixels in the optical micrograph image that were assigned to adhered particles determined before and after the adhesion testing protocol.

Before meaningful data could be obtained, background subtraction was necessary to account for ambient particles within the chamber. The continuous collection of background information during the adhesion testing protocol, as previously described enabled accurate determination of the ambient particle contributions. The background data was isolated and found to obey a simple exponential decay relationship (Eq. 9):

where *Counts(x)* represents the number of particle counts for the particle bin size of interest as a function

$$Counts(x) = A_0 + Ae^{-Bx} \quad (9)$$

of the adhesion testing protocol step, *x*. A_0 represents the initial amplitude of ambient particles, *A* is the scaling factor of the exponential decay, and *B* is the decay rate. Eq. 9 was fitted to the background data using a Microsoft® Excel® Solver add-in. The parameters determined from this fitting were then used to subtract the background contributions to the experimental steps that involved activation of the sonic wand. An example of this separation and subtraction process is shown below (Figure 4).

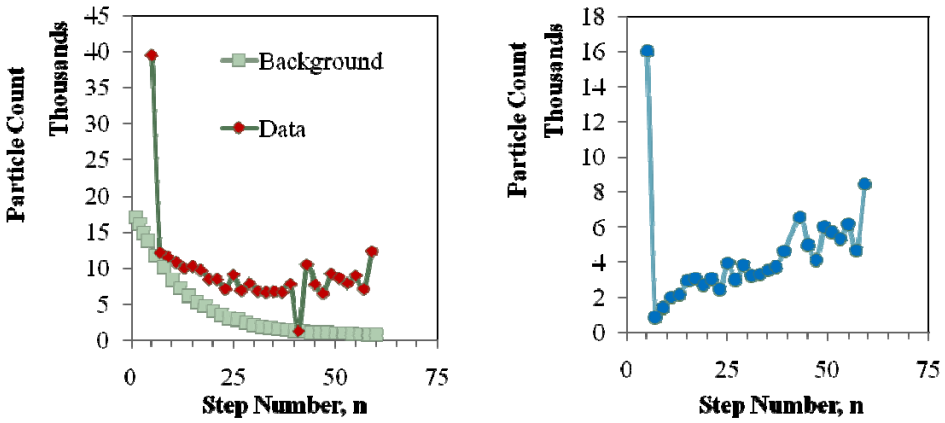

Figure 4. (A) The background data collected before, after, and between experimental data points. (B) The experimental data subtracted from Eq. 9 yielding optical particle counter data.

Once the cumulative count was scaled according to the $Clear_{\%}$ value (0 at start to 100 for complete clearance) and the background particulate contributions were subtracted, the surface acceleration corresponding to $Clear_{50\%}$ was recorded. For surface clearance at the end of the adhesion experimental protocol determined to be less than 100% according to Eq. 8, the surface acceleration would be adjusted appropriately. Thus, if a surface clearance was determined to be $Clear_{84\%}$, the surface acceleration would correlate to the value of $Clear_{50\%}$, not 0.5* $Clear_{84\%}$, which would correlate to $Clear_{42\%}$. An example of this is shown below for microspheres attached to the **PIS** surface (Figure 5) indicated that larger particles were removed from the surface at lower surface accelerations as a result of their larger mass generating greater detachment forces at a given acceleration. For surfaces that did not clear at least 50%, detachment data was classified as a minimal detachment force (indicating that the force required to remove the particulates from the surface was at least as large as the maximal force exerted during the adhesion testing protocol) and was computed using the maximum surface acceleration of the sonic wand tip.

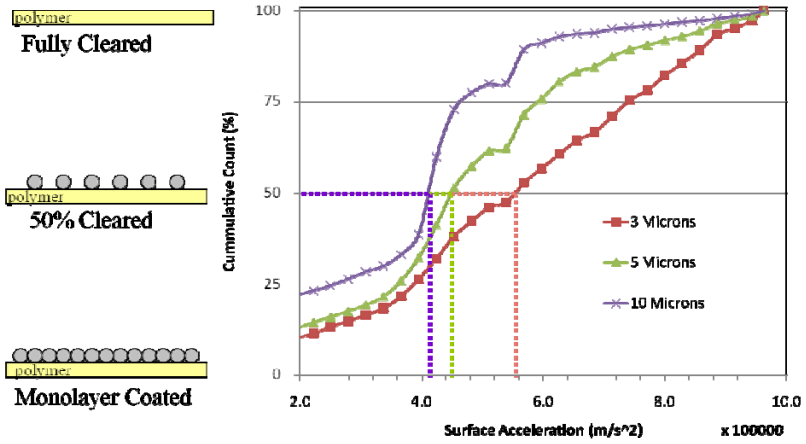

Figure 5. Surface accelerations correlating to $Clear_{50\%}$ values for 3 particle sizes.

Comparison of Detachment Force and Surface Energy:

Low surface energy materials should exhibit decreased particle adhesive interactions relative to materials with greater surface energies. Thus, it should be conceivable to correlate a material's decreased

liquid wetting (increased contact angle value) to its propensity to minimize particulate adhesion. Unfortunately, there have been few examples in the literature linking these two properties. Thus, one of the objectives in this work was to determine if such a relationship was discernable.

To compare how differences in surface energy impacted particle adhesion forces, soda-lime glass particles of discrete sizes were deposited on three different surfaces, the bare titanium alloy sonic wand tip, a commercially available polyimide (Kapton® HN), and a copoly(imide siloxane) **PIS** sample. The particle-coated surfaces were subjected to the adhesion testing protocol, and detachment force values were calculated from the collected particle count data (i.e., using the acceleration at $Clear_{50\%}$) and surface clearance analysis. The titanium alloy surface required the greatest detachment force for each particle size relative to the other two surfaces investigated in this study (Figure 6). For each material, a linear regression analysis was performed to determine the relationship between particle diameter and detachment force. The slope of the regression line was used to calculate W_a values according to the JKR adhesion force equation, Eq. 5. The **PIS** data resulted in the greatest slope (lowest W_a) indicating that this surface required significantly lower detachment forces for each of the particle sizes investigated and interpolation/extrapolation would suggest for this relationship to be maintained for other soda-lime glass particle sizes not investigated in this work.

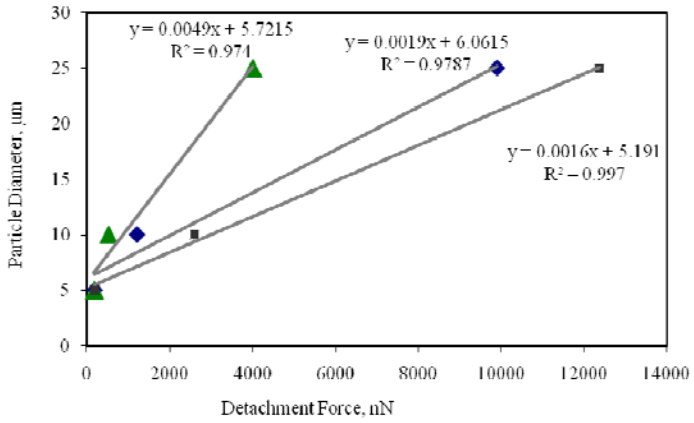

Figure 6. Detachment force values for soda-lime glass particles on copoly(imide siloxane) (triangle), Kapton® HN (diamond), and titanium (square) surfaces.

The experimentally determined W_a values were next compared to calculated W_a values derived from contact angle measurements. The work of adhesion between two dissimilar surfaces can be thermodynamically defined as:

$$W_a = \gamma_1 + \gamma_2 - \gamma_{12} \tag{10}$$

where γ_1 and γ_2 are the surface energies of the two distinct surfaces, particle and substrate respectively, and γ_{12} is the interfacial interaction energy.[34(a)] Since the interfacial interaction energy term cannot be determined using contact angle measurements, one approach to calculate the work of adhesion between surfaces is to partition the surface energy of a material into dispersive and polar contributions, γ^d and γ^p respectively, where the total surface energy, γ^{tot}, is simply the sum. Then, the work of adhesion between these surfaces is approximated as the geometric mean of these components.[36]

$$W_a = 2(\gamma_1^d \gamma_2^d)^{1/2} + 2(\gamma_1^p \gamma_2^p)^{1/2} \tag{11}$$

To calculate W_a using surface energy contributions, contact angle goniometry experiments were performed on each of the investigated surfaces with a microscope slide as a representative of the soda-lime glass particles. Contact angle values were determined on each surface using water, ethylene glycol, and methylene iodide which were used to calculate total, dispersive, and polar surface energies using the Kaelble plot according to Eq. 12.[36] The results are shown in Table 3.

$$(1+\cos\theta)\frac{\gamma_L}{2\left(\gamma_L^d\right)^{1/2}} = (\gamma_S^d)^{1/2} + (\gamma_S^p)^{1/2}\left(\frac{\gamma_L^p}{\gamma_L^d}\right)^{1/2} \tag{12}$$

Table 3. Contact angle values and surface energy parameters.

Surface	Contact Angle (°)			Surface Energy (mN m^{-1})		
	Water	Ethylene glycol	Methylene Iodide	γ^{tot}	γ^d	γ^p
Glass Slide	45	31	47	53	30	23
Titanium	63	63	54	39	25	14
Kapton® HN	85	60	49	36	33	3
Copoly(imide siloxane)	101	86	74	20	18	2

Using Eq. 11, W_a values were calculated from the surface energy parameters from Table 3. These values were then compared to the W_a values obtained from the adhesion testing device according the JKR analysis (Eq. 5). There is a clear linear relationship between the W_a values determined experimentally, using the adhesion testing device, and those derived thermodynamically, using contact angle measurements (Figure 7). To the authors' knowledge, a similar relationship has only been directly investigated in one other instance.[37] One caveat to this analysis is that although a linear trend was observed, additional electrostatic interactions resulting from highly polarized or ionic functionalities present on high surface energy material surfaces would likely result in deviation from this observed relationship.

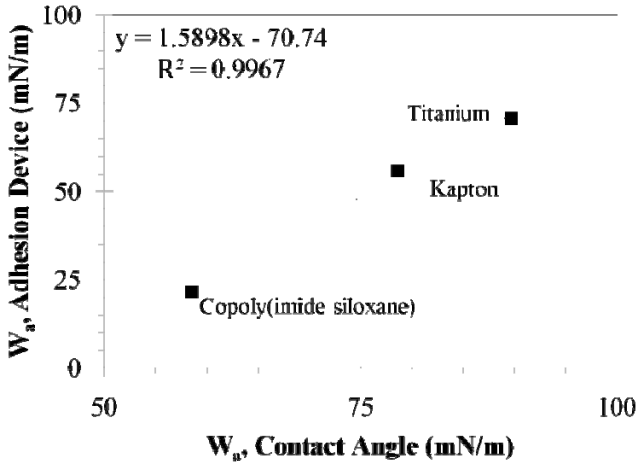

Figure 7. Comparison of W_a values determined experimentally (y-axis) and calculated using contact angle goniometry (x-axis).

Variation of Surface Topography:

The impact of surface topography on adhesive interactions was investigated by measuring the required detachment force and $Clear_{\%}$ of soda-lime glass particles on Silastic® T2 surfaces that were cured on either flat or patterned surfaces from a laser ablation patterned aluminum template. The Silastic® T2 was determined to sufficiently wet the patterned aluminum surface as indicated by optical microscopy, and exhibited topographies that were the negative of the aluminum template. Effectively, the pattern could be described as a roughened surface, on the micron and sub-micron scale, with approximately 25 μm holes arranged in a rectangular array. The generated surfaces were then coated with particulates and subjected to the adhesion test protocol to determine the detachment force and $Clear_{\%}$. As indicated in Table 4, the detachment forces required to remove the soda-lime particles from the patterned Silastic® T2 surface were dramatically reduced relative to those required on a flat surface. Similarly, the $Clear_{\%}$ values improved significantly for the patterned surfaces. Both of these results indicated that the surface topography reduced the available surface area for particle adhesion thereby reducing the required detachment force for adhered particles.

Table 4. Adhesion testing experimental results for patterned and un-patterned Silastic® T2 surfaces.

Surface	Particle Radius (μm)	Adhesion Force (μN)	$Clear_{\%}$	Contact Radius (μm)[a]
Silastic® T2	12.5	40	< 50	8.4
	20	150	< 50	15.3
Silastic® T2, patterned	12.5	6.4	75	4.6
	20	86	100	12.7

[a]*Calculated according to Eq. 6*

JKR Analysis and van der Waals Forces:

The contact radius of the adhered particles was calculated for each surface studied according to Eq. 6. Using previously described geometric relationships, the embedding depth of the adhered particles was also determined and found to be on the nanometer scale for all surfaces except the Silastic T2 surfaces, which were determined to have embedding depths as large as 35% of the particle radius. Particles adhered to the patterned Silastic T2 surface were calculated to have significant reductions in contact radii (Table 4). Molecular level origins of the adhesive interactions between particles and substrates can be investigated by calculating the contribution to the adhesion force from van der Waals interactions according to Eq. 3 (Table 5). To fully account for the adhesive interactions present in the systems investigated here, Eq. 3 would require additional scaling terms to account for surface roughness and electrostatic adhesion affects such as contact charging of particles which can increase adhesion.[38-40] However, for the purposes of this work, these additional contributions were not considered. The van der Waals contributions were calculated for adhered 25 micron soda-lime glass particles and were found to be significant for each surface studied (Table 5). Discrepancies between the calculated and experimental adhesion force values (last column in table 5) may arise from other interactions (capillary force, electrostatic interactions, etc). The magnitudes of capillary forces and electrostatic interactions are currently being investigated.

Table 5. Determination of van der Waals contribution to adhesion force values for adhered 25 μm soda-lime glass particles.

Material	H' (J)	F_{vdW} (N)	F_{adh} (N)	$F_{adh} - F_{vdW}$ (N)
Ti-6Al-4V	$1.6x10^{-19}$	$1.3x10^{-6}$	$12.0x10^{-6}$	$-6.7x10^{-7}$
Kapton®	$5.9x10^{-20}$	$4.5x10^{-6}$	$9.9x10^{-6}$	$5.4x10^{-6}$
PIS	$5.7x10^{-20}$	$4.3x10^{-6}$	$4.0x10^{-6}$	$-3.4x10^{-7}$
Silastic® T2	$5.6x10^{-20}$	$4.3x10^{-6}$	$40.0x10^{-6}$	$3.6x10^{-5}$

Conclusions

An adhesion testing device was assembled and initial results were collected to quantitatively evaluate adhesive interactions between surfaces and micron-sized particles with an emphasis towards lunar surface applications. The experimental design was organized to evaluate adhesive interactions enabling assessment of the efficacy of low surface energy materials developed for lunar dust adhesion mitigation. Optical particle counter data was collected and data processing practices implemented to obtain meaningful data relative to the sonic wand activity. Sonic wand acceleration values were determined for $Clear_{50\%}$ particle counts which were used to calculate adhesion forces. Preliminary results indicated that the adhesion force can be quantitatively determined for particulates on an array of substrates using this device. These adhesion force values were then used to calculated work of adhesion using JKR theory. A relationship between this work of adhesion values and those determined by contact angle goniometry measurements was revealed indicating that surface energy can be used as a predictive tool for adhesive interactions. Topographical modification of surfaces was also found to play a significant role in adhesive interactions with a reduction in available surface area resulting in a significant reduction in adhesion forces. Van der Waals contributions to adhesion forces were calculated and found to be less than those determined experimentally, likely due to other contributions not considered, i.e., capillary forces, electrostatic interactions, etc.

Summary and Outlook

There are a number of modifications that would engender this device with greater analytical capabilities. Implementation of a sonication device allowing both variation of the sonication amplitude and frequency would facilitate a broader variation of the investigated detachment forces. Utilization of an optical particle counter with true real-time detection capabilities would dramatically reduce the duration of a single experiment. Research is currently underway to develop integrated software systems capable of such measurements. Similarly, the use of an optical particle counter with broader, partitioned, particle size detection capabilities more closely aligned with the investigated particle sizes would lend greater confidence to the collected data. Another modification would be to house this assembly of instruments in a slightly larger environmental chamber which would allow for the sonic wand to be oriented in a vertical position relative to the optical particle counter while maintaining a position over the collection cone. This would result in all of the forces acting on adhered particles to be oriented normal to the sample plane.

The array of possible interactions between a lunar dust particle and a surface necessitates the development of different instruments oriented to investigate the impact of each interaction on adhesion strength. Although the instrument described here does not address all of the plausible contributions to adhesion, it is possible to make modifications to incorporate additional components. For example, the environmental chamber can be flushed with dry nitrogen and, with the aid of a humidity sensor, the impact of capillary forces can be addressed. Different particulate media can be utilized that better simulates lunar dust. There are several different types of lunar simulant and for the purposes of addressing particulate adhesion and contamination issues, the NASA/USGS Lunar Highlands Simulant with particle diameters less than 30 microns will be utilized.

Similarly, research is currently underway to incorporate an electric field generating device to evaluate how the presence of electric fields may impact lunar dust adhesion. Motivation to include charging affects arises from the particulate coating technique described here which may lead to contact charging of particles. In addition, the complex dynamically charged lunar environment not only contributes to the charging and transport of lunar dust, but may also influence adhesion through charge polarization interactions for sufficiently large electric fields.[41] Electric fields of magnitude ~ 1 kV/m have been predicted in lunar terminator regions and areas of sharp contrast between illuminated and shaded surfaces such as lunar craters.[42] Such regions may be preferential exploration sites because prolonged shaded regions of lunar craters may contain ice deposits[43] and therefore it is critical to generate adhesion mitigation materials that can perform effectively in such an environment. An electric field generation module has been developed and its implementation into the adhesion testing device and preliminary results are currently being evaluated.[44]

References

1. Stubbs, T., Vondrak, R., Farrell, W. (2005) Impact of Dust on Lunar Exploration, Dust in Planetary Systems, Kauai, Hawaii, United States of America, September 26-30.
2. Kobrick, R. L., Klaus, D. M. (2008) Characterizing physical properties and induced motion of lunar dust affecting surface exploration missions., 39th Lunar and Planetary Scince Conference, League City, TX, March, United States of America, 10-14.
3. Gaier, J. (2005) The Effects of Lunar Dust on EVA Systems During the Apollo Missions, National Aeronautics and Space Administration, NASA/TM-213610.
4. Gaier, J. R., Siamidis, J., Larkin, E. M. G. (2010) *Journal of Spacecraft and Rockets*, *47(1)*, pp. 147 - 152.
5. Khan-Mayberry, N. (2008) *Acta Astronautica*, *63*, pp. 1006-1014.
6. Holland, J. M., Simmonds, R. C. (1973) *Space Life Sciences*, *4*, pp. 97 - 109.
7. Taylor, L. A., Schmitt, H. H., Carrier, W. D., Nakagawa, M. (2005) The Lunar Dust Problem: From Liability to Asset, 1st Space Exploration Conference: Continuing the Voyage of Discovery, Orlando, Florida, United States of America, January 30 - February 1.
8. Lee, L.-H. (1995) *Journal of Adhesion Science and Technology*, *9(8)*, pp. 1103 - 1124.
9. Walton, O. R. (2007) Adhesion of Lunar Dust, National Aeronautics and Space Administration, NASA/CR-214685.
10. Taylor, L. A., Meek, T. T. (2005) *J. Aerospace Eng.*, *18(3)*, pp. 188 - 196.
11. Abbas, M., Tankosic, D., Craven, P., Spann, F., LeClair, A., West, E. (2007) *Planetary Space Science*, *55*, pp. 953 - 965.
12. Borisov, N., Mall, U. (2006) *Planetary Space Science*, *54*, pp. 572 - 580.
13. Stubbs, T., Vondrak, R., Farrell, W. (2006) *Advances in Space Research*, *37*, pp. 59 - 66.
14. Kolesnikov, E., Yakovlev, A. (2003) *Planetary Space Science*, *51*, pp. 879 - 885.
15. Liu, Y., Schnare, D. W., Eimer, B. C., Taylor, L. A. (2008) *Planetary Space Science*, *56*, pp. 1517-1523.
16. Kobrick, R. L., Budinski, K. G., Street Jr, K. W., Klaus, D. M. (2010) Three-body abrastion testing using lunar dust simulants to evaluate surface system materials, National Aeronautics and Space Administration, NASA/TM-216781.
17. Murphy Jr., T. W., Adelberger, E. G., Battat, J. B. R., Hoyle, C. D., McMillan, R. J., Michelsen, E. L., Samad, R. L., Stubbs, C. W., Swanson, H. E. (2010) *Icarus*, *208(1)*, pp. 31-35.
18. Wohl, C. J., Belcher, M. A., Chen, L., Connell, J. W. (2010) *Langmuir*, *26(13)*, pp. 11469-11478.

19. Gaier, J. R., Jaworske, D. A. (2007) Lunar dust on heat rejection system surfaces: problems and prospects, National Aeronautics and Space Administration, NASA/TM-214814.
20. Wilson, T. L., Wilson, K. B. (2005) Regolith sintering: a solution to lunar dust mitigation, 36th Lunar and Planetary Science Conference, League City, Texas, United States of America, March 14-18.
21. Eimer, B. C., Taylor, L. A. (2007) Dust mitigation: lunar air filtration with a permenant-magnet system (LAF-PMS), 38th Lunar and Planetary Science Conference, League City, Texas, United States of America, March 12-16.
22. Immer, C., Starnes, J., Michalenko, M., Calle, C., Mazumder, M. (2006) Electrostatic Screen for Transport of Martian and Lunar Regolith, 37th Lunar and Planetary Science Conference, League City, Texas, United States of America, March 13-17.
23. Sabri, F., Wehner, T., Hoskins, J., Schuerger, A., Hobbs, A., Barreto, J., Britt, D., Duran, R. (2008) *Advances in Space Research*, *41*, pp. 118 - 128.
24. Mullins, M., Micheals, L., Menon, V., Locke, B., Ranade, M. (1992) *Aerosol Science and Technology*, *17*, pp. 105 - 118.
25. Segeren, L., Siebum, B., Karssenberg, F., Van den Berg, J., NVancso, G. (2002) *Journal of Adhesion Science and Technology*, *16(7)*, pp. 793-828.
26. Cho, J., Lee, D., Lim, J., Cho, K., Je, J., Yi, J. (2004) *Langmuir*, *20*, pp. 10174 - 10178.
27. Ong, Q., Sokolov, I. (2007) *Journal of Colloid and Interface Science*, *310*, pp. 385-390.
28. McFarland, A. W., Poggi, M. A., Bottomley, L. A., Colton, J. S. (2005) *Journal of Micromechanics and Microengineering*, *15*, pp. 785-791.
29. Sader, J. E., Chin, J. W. M., Mulvaney, P. (1999) *Review of Scientific Instruments*, *70(10)*, pp. 3967-3969.
30. Heim, L., Kappl, M., Butt, H. (2004) *Langmuir*, *20*, pp. 2760 - 2764.
31. Zimon, A. 1969 Adhesion of Dust and Powder, Plenum Press.
32. Israelachvili, J. 2003 Intermolecular and Surface Forces, Academic Press, p. 450.
33. Zhao, Y., Shi, X., Li, W. (2003) *Reviews of Advanced Materials Science*, *5*, pp. 348 - 353.
34. (*a*) Israelachvili, J., *Intermolecular and Surface Forces*. Eds.; Academic Press: Amsterdam, 2003; p 450. (*b*) Hansen, M., Giddings, J. (1989) Analytical Chemistry, 61(8), pp. 811-819. (*c*) Sitti, M.; Fearing, R., Synthetic Gecko Foot-Hair Micro/Nano-Structures as Dry Adhesives for Future Wall-Climbing Robots. In *IEEE Robotics and Automation Conference*, Taiwan, 2003. (*d*) Dickinson, J. T., Hariadi, R. F., Scudiero, L., Langford, S. C. (1999) *Tribology Letters, 7*, pp. 113-119.
35. Carter, R. H., Huang, X., Reifsnider, K. L. (2000) Ceramic Engineering and Science Proceedings, pp.57-64.
36. Kaelble, D. H. (1970) *Journal of Adhesion*, *2(2)*, pp. 66-81.
37. Mangipudi, V.; Tirrell, M.; Pocius, A. V., Direct Measurement of Molecular Level Adhesion Between Poly(ethylene terephthalate) and Polyethylene Films: Determination of Surface and Interfacial Energies. In *Fundamentals of Adhesion and Interfaces*, Rimai, D. S.; DeMejo, L. P.; Mittal, K. L., Eds. VSP: Uthrecht, The Netherlands, 1995; p 205.
38. Jaiswal, R., Kumar, G., Kilroy, C., Beaudoin, S. (2009) *Langmuir*, *25(18)*, pp. 10612-10623.
39. Rabinovich, Y., Adler, J., Ata, A., Singh, R., Moudgil, B. (2000) *Journal of Colloid and Interface Science*, *232*, pp. 17 - 24.
40. Tang, T., Hui, C., Jagota, A. (2006) *Journal of Applied Physics*, *99*, p. 54906.
41. Jones, T. B. 1995 Force interactions between particles. In Electromechanics of Particles. Cambridge University Press, pp. 181-217.
42. Halekas, J., Lin, R., Mitchell, D. (2007) *Geophysical Research Letters*, *32*, p. L09102.

43. Sridharan, R., Ahmed, S. M., Das, T. P., Sreelatha, P., Pradeepkumar, P., Naik, N., Supriya, G. (2010) *Planetary Space Science*, *58*, pp. 947-950.
44. Wohl, C., Atkins, B., Connell, J. Design, Manufacture, and Implementation of an Electric Field Generating Device for Particulate Adhesion Testing, National Aeronautics and Space Administration, *manuscript in preparation*.

REPORT DOCUMENTATION PAGE

Form Approved
OMB No. 0704-0188

1. REPORT DATE *(DD-MM-YYYY)*	2. REPORT TYPE	3. DATES COVERED *(From - To)*
01- 02 - 2011	Technical Memorandum	

4. TITLE AND SUBTITLE

Method and Apparatus for the Quantification of Particulate Adhesion Forces on Various Substrates

5a. CONTRACT NUMBER

5b. GRANT NUMBER

5c. PROGRAM ELEMENT NUMBER

6. AUTHOR(S)

Wohl, Christopher J.; Atkins, Brad M.; Connell, John W.

5d. PROJECT NUMBER

5e. TASK NUMBER

5f. WORK UNIT NUMBER

432938.09.01.07.12

7. PERFORMING ORGANIZATION NAME(S) AND ADDRESS(ES)

NASA Langley Research Center
Hampton, VA 23681-2199

8. PERFORMING ORGANIZATION REPORT NUMBER

L-19957

9. SPONSORING/MONITORING AGENCY NAME(S) AND ADDRESS(ES)

National Aeronautics and Space Administration
Washington, DC 20546-0001

10. SPONSOR/MONITOR'S ACRONYM(S)

NASA

11. SPONSOR/MONITOR'S REPORT NUMBER(S)

NASA/TM-2011-217048

12. DISTRIBUTION/AVAILABILITY STATEMENT

Unclassified - Unlimited
Subject Category 25
Availability: NASA CASI (443) 757-5802

13. SUPPLEMENTARY NOTES

14. ABSTRACT

Mitigation strategies for lunar dust adhesion have typically been limited to qualitative analysis. This technical memorandum describes the generation and operation of an adhesion testing device capable of quantitative assessment of adhesion forces between particulates and substrates. An aerosolization technique is described to coat a surface with a monolayer of particulates. Agitation of this surface, via sonication, causes particles to dislodge and be gravitationally fed into an optical particle counter. Experimentally determined adhesion force values are compared to forces calculated from van der Waals interactions and are used to calculate the work of adhesion using Johnson-Kendall-Roberts (JKR) theory. Preliminary results indicate that a reduction in surface energy and available surface area, through topographical modification, improve mitigation of particulate adhesion.

15. SUBJECT TERMS

Lunar dust; Particle adhesion; Sonication; Surface engineering

16. SECURITY CLASSIFICATION OF:			17. LIMITATION OF ABSTRACT	18. NUMBER OF PAGES	19a. NAME OF RESPONSIBLE PERSON
a. REPORT	b. ABSTRACT	c. THIS PAGE			STI Help Desk (email: help@sti.nasa.gov)
					19b. TELEPHONE NUMBER *(Include area code)*
U	U	U	UU	21	(443) 757-5802